Calculations of Stark-broadened line shapes in phase-conjugate degenerate four-wave mixing laser spectroscopy

Krzysztof Dzierżęga*
M. Smoluchowski Institute of Physics, Jagellonian University, ulica Reymonta 4, 30-059 Kraków, Poland

Wiesław Olchawa
Institute of Physics, University of Opole, ulica Oleska 48, 45-052 Opole, Poland
(Received 8 June 2005; published 27 October 2005)

The Stark-broadened line shapes for phase-conjugate degenerate four-wave mixing (PCDFWM) laser spectroscopy are studied. The line profiles are calculated for high-density ($N_e > 10^{21}$ m^{-3}) plasma conditions and for different contributions of the Doppler broadening. Calculations are performed in the limit of low laser intensities using the perturbation approach. The theoretical model takes into account the Stark effect together with the ion dynamics, the electron collisions, and the Doppler effect. The resultant PCDFWM spectral profiles are significantly less broadened and less asymmetric than the emission profiles but shifted by similar magnitudes. Moreover, the results of our calculations show the sub-Doppler character of the PCDFWM profiles and also their strong dependence on the geometric configuration of the pump and the probe laser beams.

DOI: 10.1103/PhysRevE.72.046405 PACS number(s): 52.70.−m, 32.70.Jz, 32.60.+i, 42.65.Hw

I. INTRODUCTION

The Stark widths and shifts of spectral lines are widely studied in astrophysics and laboratory plasma physics [1]. The measurements of the Stark profiles are almost exclusively based on optical emission spectroscopy (OES) owing to its nonintrusive character and the simple experimental setup.

However, OES can provide results only for spatially integrated line intensities while the local, spatially resolved values can be deduced from the Abel inversion transformation, which may be questionable. In high-temperature environments such as plasmas the OES widths can be substantially increased by the influence of the Doppler effect. Possible corrections for the Doppler broadening require measurements of the gas temperature which can constitute a difficult task especially when the plasma is not in local thermal equilibrium. Furthermore, in dense plasmas with $N_e > 10^{21}$ m^{-3}, the strong overlap of the adjacent spectral lines can significantly disturb the measured profile.

In addition to the optical emission spectroscopy, the only other method that has been successfully used in studies of Stark profiles in dense plasmas is Doppler-free two-photon polarization spectroscopy (TPPS) which was applied to the Lyman-α [2,3] hydrogen line. Application of other laser-based methods such as saturation spectroscopy or laser-induced fluorescence to investigate line profiles in dense plasmas is very difficult. These methods, well established in the field of atomic and molecular spectroscopy, cannot be applied to the plasma studies because of the relatively high elastic and inelastic collision rates and high photon emission of the plasma. The signal to be detected with these techniques would be diminished either by velocity-changing collisions or by the nonradiative decay of the excited atoms, or would simply be masked by the plasma radiation background.

We have recently applied a phase-conjugate degenerate four-wave mixing (PCDFWM) nonlinear laser method to study the Stark profile of the 696.543 nm Ar I line in an atmospheric-pressure argon arc plasma [4]. Like TPPS, the PCDFWM method is characterized by high spatial and temporal resolutions which are determined by the overlap volume of the involved laser beams and by the temporal width of the laser pulse, respectively. PCDFWM also offers superior spectral resolution as compared to OES owing to its sub-Doppler character. The spectral resolution is further enhanced due to a strong, nonlinear dependence of the signal intensity on the detuning from the resonance frequency. Moreover, the signal beam is phase conjugated to the probe laser beam. Thus, the signal beam is highly collimated, which increases the signal-to-noise ratio and allows the signal to be readily discriminated against the plasma radiation background, in contrast to OES.

Although DFWM and TPPS are both third-order nonlinear processes, the wave mixing needs much lower (at least two orders of magnitude) laser intensities to generate a detectable signal under similar experimental conditions. This is due to the one-photon resonant nature of DFWM in contrast to the two-photon resonances occurring in TPPS. Therefore, DFWM has a much lower potential impact on the plasma state than TPPS and, at least for the laser intensities studied in this work, can be considered nonintrusive.

The standard theory of the Stark-broadened emission profile from the plasma is based on the impact and quasistatic approximations for collisions with electrons and ions, respectively [1]. This model is usually improved by inclusion of the ion dynamic effects, i.e., the effects arising from the relative motion of the ion-radiator system and leading to fluctuations of the ionic fields acting on the radiator. Unlike emission profiles, theoretical calculations of the Stark-broadened line profiles as observed with nonlinear laser

*Electronic address: krzycho@netmail.if.uj.edu.pl

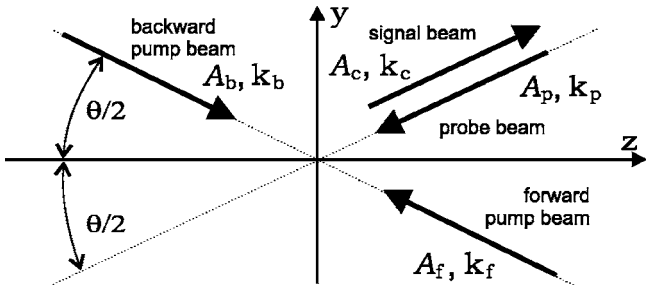

FIG. 1. Geometric configuration of PCDFWM.

spectroscopy have been the subject of only two articles concerning the plasma-broadened hydrogen Lyman-α profile in TPPS [5,6].

The aim of the present work is to calculate the line shapes of nonhydrogen radiators for the PCDFWM laser spectroscopy and taking the effect of Stark broadening into consideration. Our model takes into account all the physical processes considered also in the theory of the emission line profile: the Stark effect with ion dynamics and the Doppler effect. In addition, since the spectral features of the generated signal are affected by the geometry of the laser beams, we also study the dependence of the final line shape on the intersection angle between the probe and pump laser beams.

All calculations are performed in the limit of low laser intensities (i.e., much lower than the saturation intensity for the studied atomic transition [7,8]) using a perturbation approach. The PCDFWM line shapes obtained with our model are compared to the OES line profiles.

II. THEORY

Degenerate four-wave mixing is a nonlinear optical process involving three laser beams of identical optical frequencies which interact through the nonlinearity of a medium to generate a fourth, signal beam, at the same frequency. By analogy to holography, the DFWM signal can be understood as diffraction of one of the beams on the spatial grating of the refractive index produced by the two other incident beams.

There exist numerous geometric configurations of DFWM with the boxcar and the phase-conjugate geometry the most frequently studied. A number of theoretical papers have been devoted to DFWM phenomenon in condensed and gas-phase media. Two-level (TL) and degenerate two-level (DTL) atoms, open and closed, and homogeneously and inhomogeneously broadened systems have been investigated while interacting with laser beams of different intensities and different polarization configurations [7].

A. Model

We investigate DFWM in the phase-conjugate geometry for an open two-level radiator moving with velocity $\mathbf{v}$. We consider three plane-wave laser beams of frequency ω and of linear and parallel polarizations interacting as in Fig. 1.

The probe beam crosses the two counterpropagating (forward and backward) pump laser beams at an angle θ. The generated signal beam has the same optical frequency ω and is phase conjugated to the probe beam. In other words, it propagates backward with respect to the probe beam and its wave vector $\mathbf{k}_c$ satisfies the phase-matching relation

$$\mathbf{k}_c + \mathbf{k}_p = \mathbf{k}_f + \mathbf{k}_b. \tag{1}$$

We assume our radiator, in plasma, to undergo collisions with plasma constituents, predominantly with electrons and ions. To describe the interaction of our radiator with plasma and the incident laser beams we use the time-dependent density-matrix equations given by

$$\left(\frac{\partial}{\partial t} + \mathbf{v}\cdot\boldsymbol{\nabla}\right)\rho_{11} = -\gamma_1\rho_{11} - \frac{i}{\hbar}(V_{12}\rho_{21} - V_{21}\rho_{12}) + \Lambda_1, \tag{2a}$$

$$\left(\frac{\partial}{\partial t} + \mathbf{v}\cdot\boldsymbol{\nabla}\right)\rho_{22} = -\gamma_2\rho_{22} + \frac{i}{\hbar}(V_{12}\rho_{21} - V_{21}\rho_{12}) + \Lambda_2, \tag{2b}$$

$$\left(\frac{\partial}{\partial t} + \mathbf{v}\cdot\boldsymbol{\nabla}\right)\rho_{21} = -(i\omega(F) + \gamma)\rho_{21} - \frac{i}{\hbar}V_{21}(\rho_{11} - \rho_{22}). \tag{2c}$$

The diagonal matrix elements ρ_{11} and ρ_{22} are proportional to the populations of the lower (1) and the upper (2) levels while the off diagonal elements $\rho_{12}=\rho_{21}^*$ describe the optical coherences between these levels. The interaction potential V_{12} between the radiator and the laser beams in the rotating wave approximation is given by

$$V_{12}(\mathbf{r},t) = -\boldsymbol{\mu}_{12}\cdot\mathbf{E}(\mathbf{r},t) = -\frac{1}{2}\mu_{12}\sum_n A_n e^{-i(\omega t - \mathbf{k}_n\cdot\mathbf{r})}, \tag{3}$$

where μ_{12} is the dipole moment of the atom, and A_n and $\mathbf{k}_n$ $(n=f,b,p)$ are the amplitude and the wave vector of the nth optical field. γ_1 and γ_2 stand for the population decay rates while the dephasing rate γ corresponds to the electron impact broadening which is directly proportional to the electron number density N_e. In the absence of laser beams both levels are populated at pump rates Λ_1 and Λ_2.

The interaction of the radiator with surrounding particles not only affects its decay rates but also modifies its transition frequency. In order to describe this effect we introduce the transition frequency $\omega(F)$ defined as for the emission profiles in plasma [1]:

$$\omega(F) = \omega_0 + d_{el} - CF^2,$$

where ω_0 is the free-space, transition frequency of the radiator. The second and third terms correspond to the frequency shifts due to collisions with electrons and to the quadratic Stark effect experienced by the nonhydrogen radiator exposed to the ion microfield $\mathbf{F}$, respectively. The Stark constant $C=\gamma\alpha^{4/3}/F_0^2$ where the static ion broadening parameter α is proportional to $N_e^{1/4}$ and is defined for instance in [1]. The quantity $F_0=\left(\frac{4}{15}\right)^{2/3}2\pi eN_e^{2/3}$ is the Holtsmark normal field related to the distribution function of the electric field magnitudes in plasma.

B. Calculations of the PCDFWM signal intensity

For given velocity $\mathbf{v}$ of the radiator and the magnitude F of the ion microfield, the solutions to Eqs. (2) can be written in the form

$$\rho_{11}(\mathbf{r},t;\mathbf{v},F) = \sum_q \sigma_{11}(t,\mathbf{k}_q;\mathbf{v},F)e^{i\mathbf{k}_q\cdot\mathbf{r}} \equiv \sum_q \sigma_{11}(\mathbf{k}_q)e^{i\mathbf{k}_q\cdot\mathbf{r}} \tag{4}$$

for populations and

$$\rho_{21}(\mathbf{r},t;\mathbf{v},F) = \sum_q \sigma_{21}(t,\mathbf{k}_q;\mathbf{v},F)e^{-i(\omega t-\mathbf{k}_q\cdot\mathbf{r})} \equiv \sum_q \sigma_{21}(\mathbf{k}_q)e^{-i(\omega t-\mathbf{k}_q\cdot\mathbf{r})} \tag{5}$$

for coherences where σ_{ij} are slowly varying quantities. The various wave vectors $\mathbf{k}_q$ are determined by linear combinations of $\mathbf{k}_f$, $\mathbf{k}_b$, and $\mathbf{k}_p$. The last expressions introduce the abbreviated notations for the density matrix elements $\sigma_{nm}(\mathbf{k}_q)$, which will be used henceforth.

The system of Eqs. (2) cannot be solved analytically so we use the perturbation theory and limit our solution to the third-order terms which are the lowest terms to describe generation of the PCDFWM signal. In other words, the solution is correct for the case of low laser intensities with respect to the saturation intensity.

In order to solve Eqs. (2) in terms of a perturbation expansion, we replace the interaction potential by

$$V_{12} = \lambda\ V_{12}, \tag{6}$$

where λ is a parameter varying from zero to unity. Then we seek a solution to the matrix equations in the form of a power series in λ:

$$\sigma_{nm} = \sigma_{nm}^{(0)} + \lambda\sigma_{nm}^{(1)} + \lambda^2\sigma_{nm}^{(2)} + \lambda^3\sigma_{nm}^{(3)} + \cdots. \tag{7}$$

Introducing Eqs. (4)–(7) into Eqs. (2) and requiring all terms proportional to $\lambda^{(N)}$ to satisfy separately the equality we obtain the following set of equations:

$$\dot{\sigma}_{11}^{(0)}(0) = -\gamma_1\sigma_{11}^{(0)}(0) + \Lambda_1, \tag{8a}$$

$$\dot{\sigma}_{22}^{(0)}(0) = -\gamma_2\sigma_{22}^{(0)}(0) + \Lambda_2, \tag{8b}$$

$$\dot{\sigma}_{21}^{(1)}(\mathbf{k}_f) = \{i[\omega-\omega(F)-\mathbf{k}_f\cdot\mathbf{v}]-\gamma\}\sigma_{21}^{(1)}(\mathbf{k}_f) + \frac{i\mu_{21}A_f}{2\hbar}[\sigma_{11}^{(0)}(0)-\sigma_{22}^{(0)}(0)], \tag{8c}$$

$$\dot{\sigma}_{21}^{(1)}(\mathbf{k}_b) = \{i[\omega-\omega(F)-\mathbf{k}_b\cdot\mathbf{v}]-\gamma\}\sigma_{21}^{(1)}(\mathbf{k}_b) + \frac{i\mu_{21}A_b}{2\hbar}[\sigma_{11}^{(0)}(0)-\sigma_{22}^{(0)}(0)], \tag{8d}$$

$$\dot{\sigma}_{12}^{(1)}(\mathbf{k}_p) = \{-i[\omega-\omega(F)-\mathbf{k}_p\cdot\mathbf{v}]-\gamma\}\sigma_{12}^{(1)}(\mathbf{k}_p) - \frac{i\mu_{12}A_p}{2\hbar}[\sigma_{11}^{(0)}(0)-\sigma_{22}^{(0)}(0)], \tag{8e}$$

$$\dot{\sigma}_{11}^{(2)}(\mathbf{k}_f-\mathbf{k}_p) = -[i(\mathbf{k}_f-\mathbf{k}_p)\cdot\mathbf{v}+\gamma_1]\sigma_{11}^{(2)}(\mathbf{k}_f-\mathbf{k}_p) + \frac{i\mu_{12}A_p}{2\hbar}\sigma_{21}^{(1)}(\mathbf{k}_f) - \frac{i\mu_{21}A_f}{2\hbar}\sigma_{12}^{(1)}(\mathbf{k}_p), \tag{8f}$$

$$\dot{\sigma}_{11}^{(2)}(\mathbf{k}_b-\mathbf{k}_p) = -[i(\mathbf{k}_b-\mathbf{k}_p)\cdot\mathbf{v}+\gamma_1]\sigma_{11}^{(2)}(\mathbf{k}_b-\mathbf{k}_p) + \frac{i\mu_{12}A_p}{2\hbar}\sigma_{21}^{(1)}(\mathbf{k}_b) - \frac{i\mu_{21}A_b}{2\hbar}\sigma_{12}^{(1)}(\mathbf{k}_p), \tag{8g}$$

$$\dot{\sigma}_{22}^{(2)}(\mathbf{k}_f-\mathbf{k}_p) = -[i(\mathbf{k}_f-\mathbf{k}_p)\cdot\mathbf{v}+\gamma_2]\sigma_{22}^{(2)}(\mathbf{k}_f-\mathbf{k}_p) - \frac{i\mu_{12}A_p}{2\hbar}\sigma_{21}^{(1)}(\mathbf{k}_f) + \frac{i\mu_{21}A_f}{2\hbar}\sigma_{12}^{(1)}(\mathbf{k}_p), \tag{8h}$$

$$\dot{\sigma}_{22}^{(2)}(\mathbf{k}_b-\mathbf{k}_p) = -[i(\mathbf{k}_b-\mathbf{k}_p)\cdot\mathbf{v}+\gamma_2]\sigma_{22}^{(2)}(\mathbf{k}_b-\mathbf{k}_p) - \frac{i\mu_{12}A_p}{2\hbar}\sigma_{21}^{(1)}(\mathbf{k}_b) + \frac{i\mu_{21}A_b}{2\hbar}\sigma_{12}^{(1)}(\mathbf{k}_p), \tag{8i}$$

$$\dot{\sigma}_{21}^{(3)}(\mathbf{k}_c) = \{i[\omega-\omega(F)+\mathbf{k}_p\cdot\mathbf{v}]-\gamma\}\sigma_{21}^{(3)}(\mathbf{k}_c) + \frac{i\mu_{21}A_f}{2\hbar}[\sigma_{11}^{(2)}(\mathbf{k}_b-\mathbf{k}_p)-\sigma_{22}^{(2)}(\mathbf{k}_b-\mathbf{k}_p)] + \frac{i\mu_{21}A_b}{2\hbar}[\sigma_{11}^{(2)}(\mathbf{k}_f-\mathbf{k}_p)-\sigma_{22}^{(2)}(\mathbf{k}_f-\mathbf{k}_p)]. \tag{8j}$$

The PCDFWM signal is determined by the phase-matched component $\sigma_{21}^{(3)}(\mathbf{k}_c)e^{-i(\omega t-\mathbf{k}_c\cdot\mathbf{r})}$ of the total coherence with $\mathbf{k}_c=-\mathbf{k}_p$ according to Eq. (1). The system of Eqs. (8) includes only these equations which are coupled (directly or indirectly) with the PCDFWM component. The spectral profile $I(\omega)$ of the PCDFWM signal intensity at a large distance s from the interaction region and in the dipole approximation is given as (cf. [7])

$$I(\omega) = \frac{1}{4\pi s^2}\frac{ck^4V^2}{2\pi\epsilon_0}\left|\int_0^\infty \langle\mu_{12}\sigma_{21}^{(3)}(\mathbf{k}_c)\rangle_{\mathbf{v},\mathbf{F}}dt\right|^2. \tag{9}$$

$\langle\cdots\rangle_{\mathbf{v},\mathbf{F}}$ denotes an average over radiator velociy and ionic microfield distribution functions, and V stands for the volume of the interaction region.

C. Calculation of the influence of the ion microfields

The fundamental contribution to the linewidth of the nonhydrogenic radiators which results from interaction with ion microfields can be treated within the quasistatic approximation. The ion dynamics effect arising from the relative motion of the radiator-ion system and leading to slow fluctuations of the ionic fields gives only a small ($<10\%$) contribution to the ionic broadening and in principle can be neglected. However, we decided to include this effect into our model in order to estimate its influence on the DFWM line profile. Calculations were performed using the model microfield method (MMM) [9] which is relatively simple and does not require simulations. The accuracy of this method was studied in [10] where the authors claim that by

interpolation between the ion impact and quasistatic limits, the MMM was able to account for the ion dynamics effects.

In the matrix notation, Eqs. (8) can be written in the form

$$\dot{\boldsymbol{\sigma}} = \mathbf{M}\boldsymbol{\sigma} + \boldsymbol{\Lambda}, \tag{10}$$

where the vector $\boldsymbol{\sigma}$ is

$$\begin{aligned}\boldsymbol{\sigma} = \{&\sigma_{11}^{(0)}(0), \sigma_{22}^{(0)}(0), \sigma_{21}^{(1)}(\mathbf{k}_f), \sigma_{21}^{(1)}(\mathbf{k}_b), \sigma_{12}^{(1)}(\mathbf{k}_p),\\ &\times\sigma_{11}^{(2)}(\mathbf{k}_n - \mathbf{k}_m), \sigma_{11}^{(2)}(\mathbf{k}_b - \mathbf{k}_p), \sigma_{22}^{(2)}(\mathbf{k}_f - \mathbf{k}_p),\\ &\times\sigma_{22}^{(2)}(\mathbf{k}_b - \mathbf{k}_p), \sigma_{21}^{(3)}(\mathbf{k}_c)\}^{\mathrm{T}}.\end{aligned}$$

Within the MMM theory, the time separation between successive jumps of the ion microfield follows a Poisson distribution law with density $\nu(F)$ which is a function of the microfield value F [11]

$$\begin{aligned}\nu(F) = \frac{\omega_{pi}}{1+x}\Bigg\{&\left(\frac{40x}{Z_i}\right)^{1/5}\left(\frac{1}{1+Z_i}\right)^{1/10}\\ &+ x\left[\left(\frac{x+1}{Z_i}\right)\left(\frac{1}{1+Z_i}\right)^{1/2} + \frac{3}{2}\sqrt{\pi/2}\right]\Bigg\},\end{aligned}$$

$$x = \frac{1}{x_0}\int_0^F F' W(F') dF',$$

$$x_0 = \left(\frac{18}{\pi}\right)^{1/2}\left(\frac{4e^2 N_e (2\pi)^{3/2}}{15\lambda_D}\right), \tag{11}$$

where Z_i is the charge of the perturbing ion, ω_{pi} is the ion plasma frequency, and λ_D is the Debye length.

The calculation of the time integral of σ, averaged over all the realizations of the ionic microfields $\mathbf{F}$, can be expressed as [9]

$$\begin{aligned}\{\sigma\}_{MMM} &= \int_0^\infty \sigma_{MMM}(t) dt\\ &= [\{T(i\nu)\} + \{\nu T(i\nu)\}\{\nu\mathbf{I} - \nu^2 T(i\nu)\}^{-1}\{\nu T(i\nu)\}]\boldsymbol{\Lambda},\end{aligned} \tag{12}$$

where $\mathbf{I}$ is the unity matrix, the pumping vector $\boldsymbol{\Lambda} = (\Lambda_1, \Lambda_2, 0, 0, 0, 0, 0, 0, 0, 0)^{\mathrm{T}}$, and $T(i\nu)$ is the Laplace transform of the evolution operator $T(t)$ in the Louville space equal to

$$T(i\nu) = (\nu\mathbf{I} - \mathbf{M})^{-1}. \tag{13}$$

The brace brackets $\{\cdots\}$ denote averaging over the static field distribution function $W(\mathbf{F})$ [12],

$$\{\cdots\} = \int_0^\infty (\cdots) W(\mathbf{F}) d\mathbf{F}. \tag{14}$$

The calculation of the operator $\{T(i\nu)\}$ involves separation of the $\mathbf{M}$ matrix into its diagonal (D) and off-diagonal (B) parts and then expansion of Eqs. (12) and (13) in powers of B up to the third-order terms. Finally, we find the spectral distribution of the PCDFWM signal intensity to be expressed by

$$I(\omega) \sim |\langle (0,0,0,0,0,0,0,0,0,0,1)\{T^{(3)}\}_{MMM}\boldsymbol{\Lambda}\rangle_{\mathbf{v}}|^2, \tag{15}$$

with

$$\begin{aligned}\{T^{(3)}\}_{MMM} = &\{T^{(3)}\} + \{\nu T^{(0)}\}T'^{(3)}\{\nu T^{(0)}\} + \{\nu T^{(1)}\}T'^{(2)}\{\nu T^{(0)}\}\\ &+ \{\nu T^{(0)}\}T'^{(2)}\{\nu T^{(1)}\} + \{\nu T^{(2)}\}T'^{(1)}\{\nu T^{(0)}\}\\ &+ \{\nu T^{(1)}\}T'^{(1)}\{\nu T^{(1)}\} + \{\nu T^{(0)}\}T'^{(1)}\{\nu T^{(2)}\}\\ &+ \{\nu T^{(3)}\}T'^{(0)}\{\nu T^{(0)}\} + \{\nu T^{(2)}\}T'^{(0)}\{\nu T^{(1)}\}\\ &+ \{\nu T^{(1)}\}T'^{(0)}\{\nu T^{(2)}\} + \{\nu T^{(0)}\}T'^{(0)}\{\nu T^{(3)}\},\end{aligned} \tag{16}$$

$$T^{(0)} = (\nu I - D)^{-1}, \tag{17a}$$

$$T^{(1)} = T^{(0)} B T^{(0)}, \tag{17b}$$

$$T^{(2)} = T^{(0)} B T^{(0)} B T^{(0)}, \tag{17c}$$

$$T^{(3)} = T^{(0)} B T^{(0)} B T^{(0)} B T^{(0)}, \tag{17d}$$

and

$$T'^{(0)} = \{\nu I - \nu^2 T^{(0)}\}^{-1}, \tag{18a}$$

$$T'^{(1)} = T'^{(0)}\{\nu^2 T^{(1)}\}T'^{(0)}, \tag{18b}$$

$$T'^{(2)} = T'^{(0)}\{\nu^2 T^{(1)}\}T'^{(0)}\{\nu^2 T^{(1)}\}T'^{(0)} + T'^{(0)}\{\nu^2 T^{(2)}\}T'^{(0)}, \tag{18c}$$

$$\begin{aligned}T'^{(3)} = &T'^{(0)}\{\nu^2 T^{(3)}\}T'^{(0)} + T'^{(0)}\{\nu^2 T^{(1)}\}T'^{(0)}\{\nu^2 T^{(2)}\}T'^{(0)}\\ &+ T'^{(0)}\{\nu^2 T^{(2)}\}T'^{(0)}\{\nu^2 T^{(1)}\}T'^{(0)}\\ &+ T'^{(0)}\{\nu^2 T^{(1)}\}T'^{(0)}\{\nu^2 T^{(1)}\}T'^{(0)}\{\nu^2 T^{(1)}\}T'^{(0)}.\end{aligned} \tag{18d}$$

The angular brackets $\langle\cdots\rangle_{\mathbf{v}}$ denote averaging over the radiator velocity distribution function which is supposed to be Maxwellian. By setting $\mathbf{F}=0$ and $\mathbf{v}=0$ in Eqs. (8) we recover the results for the PCDFWM signal intensity obtained in [8].

III. RESULTS AND DISCUSSION

In the preceding section we have derived an expression for the PCDFWM signal intensity for laser beams with equal amplitude in the limit of low intensity, which is low with respect to the saturation intensity of the investigated transition. Our result will now be used to study the spectral characteristics of the PCDFWM signal depending on the geometry of the laser beams, the Doppler broadening, and the ionic microfields. These characteristics are of great practical importance when we consider the application of PCDFWM laser spectroscopy to study the Stark profiles of spectral lines in plasmas. In our calculations the quasistatic broadening is supposed to be a significant contribution to the electronic broadening. In practice, this means that we consider plasmas with $N_e > 10^{21}$ m^{-3} and $T > 10\,000$ K. In the following, all calculations are performed for He as the radiator, which is the simplest system undergoing the quadratic Stark effect and which experiences relatively large Doppler broadening.

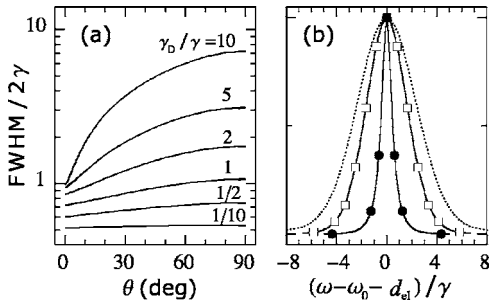

FIG. 2. (a) Angular dependence of the PCDFWM signal linewidth (FWHM) calculated for different contributions of the Doppler broadening (γ_D/γ). (b) Spectral line shapes of the PCDFWM signals (continuous lines) calculated for $\gamma_D/\gamma=5$ and $\theta=0°$ (●) and 90° (□) and the emission profile (dotted line) for comparison.

A. Angular dependence of the PCDFWM line shape

In this section we analyze the influence of the Doppler broadening (γ_D) on the PCDFWM line shape for different angles θ between the pump and the probe laser beams.

Figures 2(a) and 2(b) show the results of our numerical calculations of the PCDFWM line shapes neglecting the ion microfield effect ($\alpha=0$). Figure 2(a) shows the angular dependence of the full width at half maximum (FWHM) determined for radiators with different Doppler broadening contribution. For a homogeneously broadened medium ($\gamma_D \ll \gamma$) the terms of the kind $(\mathbf{k}_i-\mathbf{k}_j)\cdot\mathbf{v}$ in Eqs. (8) are of minor importance, and hence the spectral profile of the PCDFWM signal is nearly independent of the angular configuration of the laser beams. It also reveals a highly subhomogeneous character with FWHM of 1.02γ in the collinear configuration of the laser beams. In the opposite case, when the medium is inhomogeneously broadened ($\gamma_D \gg \gamma$), the profile of PCDFWM shows strong angular dependence and its FWHM varies from about 2γ at $\theta=0°$ to a value of the order of $2\gamma_D$ at $\theta=90°$. For the purpose of comparison, in Fig. 2(b), we present the PCDFWM line shapes calculated in the case of $\gamma_D/\gamma=5$ and for $\theta=0°$ and 90° together with the emission profile.

The angular dependence of the PCDFWM signal originates from the motion of the radiator and is basically due to two physical processes. The first is the effect of population grating destruction due to thermal motion of the investigated radiators and the second is the signal decrease due to frequency detuning from the resonance frequency by the Doppler effect.

DFWM in two-level systems is usually interpreted in terms of the spatial population gratings which lifetime equals the population lifetime $\tau=\gamma_1^{-1}+\gamma_2^{-1}$. These gratings are formed through the interference of two laser beams. Subsequent diffraction of the third laser beam leads to the signal beam generation. There are two contributions to the signal: (i) diffraction of the field A_b by the grating formed by $A_f A_p^*$ and (ii) diffraction of the field A_f by the grating formed by $A_b A_p^*$. These two gratings are formed in mutually perpendicular directions with modulation periods

$$D_{fp}=2\pi/|\mathbf{K}_{fp}| \equiv 2\pi/|\mathbf{k}_f-\mathbf{k}_p|=\lambda/2\,\sin(\theta/2), \quad (19a)$$

$$D_{bp}=2\pi/|\mathbf{K}_{bp}| \equiv 2\pi/|\mathbf{k}_b-\mathbf{k}_p|=\lambda/2\,\cos(\theta/2). \quad (19b)$$

When θ increases from 0 to $\pi/2$ the grating periods D_{fp} and D_{bp} vary from ∞ to $\lambda/\sqrt{2}$ and from $\lambda/2$ to $\lambda/\sqrt{2}$, respectively. The significance of the grating washout is measured by the mean free path $l \simeq \langle v\rangle\tau$ which the radiator travels with the average thermal speed $\langle v\rangle$ during the population grating lifetime τ compared to the spatial period of the grating $D_{f(b)p}$. It follows that the grating washout is caused by atoms moving perpendicularly to the grating planes over a distance l longer than the period of the grating.

In the collinear configuration of the laser beams D_{fp} becomes infinite and the largest number of atoms gives rise to the signal. When θ increases, D_{fp} rapidly decreases with D_{bp} almost constant and so a lower number of atoms can contribute.

The second effect results from the velocity selection by laser beams due to the Doppler effect. The laser beams interact with velocity groups defined with respect to directions of $\mathbf{k}_j$. For the collinear configuration velocity selection is made along one direction. At resonance, only a group of atoms with velocity components such that $|kv| < \gamma$ are selected to interact with all laser beams and hence the resultant profile is Doppler-free. When θ increases the velocity selection is now in two dimensions. In the direction of the pump beams still the same groups of atoms are selected. However, in the perpendicular direction, the probe beam selects atoms with velocities depending on the laser detuning from the resonance. This implies a line shape with non-negligible Doppler broadening contribution increasing with the angle θ.

The effects described above act simultaneously and cannot be separated. They affect both the amplitude and the line shape of the signal.

The same problem of the angular dependence of DFWM signals was studied by Wandzura [13], Bloch and Ducloy [14], and recently by de Oliveira and Rios Leite [15]. Their results are consistent with our results; however, they treat only the case of the inhomogeneously broadened medium.

In order to evaluate the significance of the geometric configuration of the laser beams in measurements of the Stark profiles we calculated the PCDFWM line shapes assuming the atomic and plasma parameters such as observed in laboratory plasmas. We assumed a typical electron impact (homogeneous) broadening $\gamma=5.2\times10^{11}$ s^{-1} ($\Delta\lambda=0.1$ nm, $\lambda=600$ nm) at $N_e=10^{22}$ m^{-3} and $T=10\,000$ K and we neglected the ionic effects ($\alpha=0$). Finally, at the above plasma conditions $\gamma_D \cong \gamma$.

Figure 3 presents the FWHM of the PCDFWM and the emission line profiles at constant $T=10\,000$ K and depending on the electron number density. At electron densities $N_e \gg 10^{22}$ m^{-3} the linewidth becomes independent of the geometric configuration. On the other hand, for $N_e \ll 10^{22}$ m^{-3}, the linewidth increases with θ due to the large contribution of the Doppler effect.

Our calculations show an important influence of the geometric configuration of the laser beams on the PCDFWM line profile as long as the Doppler broadening is significant.

B. Ion microfields

In the plasma, interaction of the radiator with surrounding ions results in shifted and asymmetrically broadened emis-

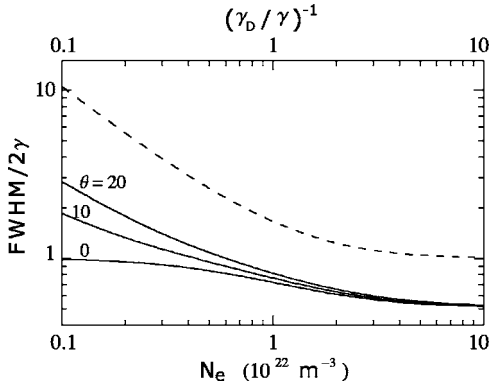

FIG. 3. Dependence of the PCDFWM (continuous lines) and the emission (broken line) linewidths (FWHM) on the electron number density N_e. Calculations were performed neglecting the ion effects ($\alpha=0$) and assuming the electron impact (homogeneous) broadening $\gamma=5.2\times10^{11}$ s^{-1} ($\Delta\lambda=0.1$ nm, $\lambda=600$ nm) at $N_e=10^{22}$ m^{-3} and $T=10\,000$ K. At the given plasma parameters we also assumed $\gamma_D=\gamma$.

sion line profiles. The similar effects are also expected in the case of the PCDFWM line profiles. The significance of the ion microfield effects has been commonly measured by the static ion broadening parameter α. In the case of a typical arc plasma with electron density $N_e>10^{22}$ m^{-3} and temperature $T>10\,000$ K α varies from 0.01 to 1.5 for most of the spectral lines [1].

In Fig. 4 we show the emission and the PCDFWM line profiles calculated including the ion microfield effects. The calculations were performed assuming $\alpha=0.2$ at $N_e=10^{22}$ m^{-3} and $T=T_i=20\,000$ K where T_i stands for the ion temperature. Moreover, we assume the homogeneous (electron impact) broadening $\gamma=5.2\times10^{11}$ s^{-1} ($\Delta\lambda=0.1$ nm at $\lambda=600$ nm) for given electron density and temperatures and $\theta=20°$ as the intersection angle between the probe and the pump lasers beams.

Although the PCDFWM profile is substantially narrower than the emission profile, they are shifted by a similar magnitude by the ion microfields.

Since under the real experimental conditions the separation of the total line shift into the ion and the electron contributions is impossible, the line shift is not an appropriate parameter to be measured experimentally in studies of the

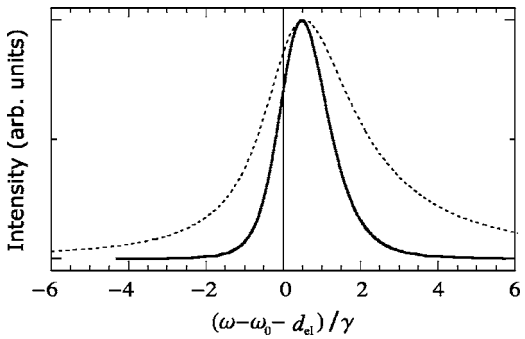

FIG. 4. The PCDFWM (continuous line) and the emission (broken line) profiles calculated for $\alpha=0.2$, $N_e=10^{22}$ m^{-3}, $T=T_i=20\,000$ K, and $\theta=20°$.

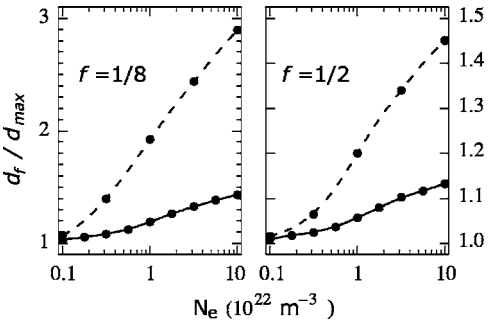

FIG. 5. Asymmetry of the PCDFWM (continuous lines) and the emission (broken lines) line shapes determined at $f=1/2$ and $1/8$ depending on the electron density. Calculations performed assuming $\alpha=0.2$ (at $N_e=10^{22}$ m^{-3}) and constant $T=T_i=20\,000$ K and $\theta=20°$.

ion microfield effects. Instead, asymmetry of the line profile can be investigated. Asymmetry of the line profile is usually defined as the ratio of the shift of the line center (d_f) measured at some height (f) of the line to the shift of the maximum (d_{max}) of the line. Figure 5 shows the asymmetries of the emission and the PCDFWM line profiles measured at one-half ($f=1/2$) and at one-eighth ($f=1/8$) of the maximum of the line profile depending on the electron number density at constant temperatures $T=T_i=20\,000$ K. Our calculations were made assuming $\alpha=0.2$, $\gamma=5.2\times10^{11}$ s^{-1} at $N_e=10^{22}$ m^{-3} and $\theta=20°$. One can notice a much larger asymmetry for the emission profiles than for the PCDFWM profiles. In both cases the lower the f values, the larger is the asymmetry observed.

The relative motion of the ion-radiator system leads to fluctuations of ionic microfields acting on the radiator. These fluctuations lead to additional broadening of the investigated line profiles. The influence of the ion dynamics effects on the final profiles was studied with respect to the quasistatic case, which corresponds to $T_i=0$ in our calculations.

Figure 6 shows the ion-temperature dependence of the total width (FWHM) of the PCDFWM and the emission profiles with relation to FWHM_{qs} of the appropriate profiles calculated within the quasistatic approximation. These calculations were performed for the physical conditions indicated in Fig. 4.

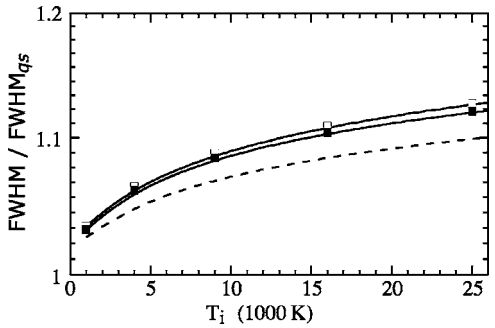

FIG. 6. The contribution of the ion dynamics effect to the total linewidth (FWHM) of the PCDFWM (continuous line) and the emission (broken line) profiles. Evaluations made with respect to the quasistatic case (FWHM_{qs}). Calculations performed for $\alpha=0.2$ (at $N_e=10^{22}$ m^{-3}), $T=20\,000$ K, and $\theta=0°$ (■) and 90° (□).

The contribution of the ion dynamics to the total width of the line profiles is slowly increasing with T_i and is only weakly dependent on the geometrical configuration of the laser beams. This kind of line broadening is expected, as the ions become more impacted. However, this effect does not change either the shift or the asymmetry of the line profile.

IV. SUMMARY AND CONCLUSIONS

The plasma-broadened Stark profiles for phase-conjugate degenerate four-wave mixing laser spectroscopy were calculated. The line profiles were calculated for a two-level radiator within the density-matrix formalism and in the limit of low laser intensities using the perturbation approach. The theoretical model of the PCDFWM spectral profile in plasma took into account the contribution of the Stark effect together with the ion dynamics and the Doppler effect as well as the geometrical configuration of the laser beams. Calculations were performed for high-density ($N_e > 10^{21}$ m^{-3}) and low-temperature ($T, T_i \approx 10\,000$ K) plasma conditions.

Although the PCDFWM spectral profiles are significantly less broadened than the emission profiles, they both shift by a similar magnitude. The asymmetry due to the static ion broadening is less pronounced through the PCDFWM profile than through the emission profile. In addition, in both cases the ion dynamics effects play only a minor role. The wings of the DFWM profile are substantially suppressed, which reduces the potential influence of the adjacent lines on the measured profile.

Another essential feature of the PCDFWM spectroscopy is a significant reduction of the Doppler broadening, provided that the laser beams are not too far from the collinear configuration. In the case of negligible ionic and Doppler broadening with respect to the electronic broadening one can write $\mathrm{FWHM}_{emission} \approx 2 \times \mathrm{FWHM}_{PCDFWM}$.

This method, providing high spectral and spatial resolution, can serve as a nonintrusive and complementary or alternative method for spectroscopic investigations of the Stark profiles of nonresonance lines in dense plasmas using commercially available pulsed visible dye lasers.

The simple model of the two-level radiator interacting with plasma constituents presented in this paper is valid only in the case of laser beams with linear and parallel polarizations. A model that includes the level degeneracy and laser beams with arbitrary polarizations is currently under study and is planned to be the subject of a future paper.

ACKNOWLEDGMENT

K.D. wishes to acknowledge the partial support of this work by the Polish Ministry of Scientific Research and Information Technology Grant No. 1PO3B09026.

[1] H. R. Griem, *Spectral Line Broadening by Plasmas* (Academic, New York, 1974).
[2] K. Danzmann, K. Grützmacher, and B. Wende, Phys. Rev. Lett. **57**, 2151 (1986).
[3] A. Steiger, Phys. Scr., T **86**, 68 (2000).
[4] K. Dzierżęga, Ł. Bratasz, S. Pellerin, B. Pokrzywka, and K. Musioł, Phys. Scr. **67**, 52 (2003).
[5] J. Seidel, Phys. Rev. Lett. **57**, 2154 (1986).
[6] M. A. Gigosos and M. A. González, Phys. Rev. E **58**, 4950 (1998).
[7] R. T. Bratfalean, G. M. Lloyd, and P. Ewart, J. Opt. Soc. Am. B **16**, 952 (1999), and references therein.
[8] R. L. Abrams, J. F. Lam, R. C. Lind, D. G. Steel, and P. F. Liao, *Optical Phase Conjugation* (Academic, New York, 1983).
[9] A. Brissaud and U. Frisch, J. Quant. Spectrosc. Radiat. Transf. **11**, 1767 (1971).
[10] S. Alexiou, P. Sauvan, A. Poquérusse, E. Leboucher-Dalimier, and R. W. Lee, Phys. Rev. E **59**, 3499 (1999).
[11] C. Stehlé, Astron. Astrophys. Trans. **292**, 699 (1994).
[12] J. Halenka, Z. Phys. D: At., Mol. Clusters **16**, 1 (1990).
[13] S. M. Wandzura, Opt. Lett. **4**, 208 (1979).
[14] M. Ducloy and D. Bloch, J. Phys. (France) **42**, 711 (1981).
[15] P. C. de Oliveira and J. R. Rios Leite, Appl. Phys. B: Lasers Opt. **67**, 601 (1998).